International Journal of Minerals, Metallurgy and Materials
Volume 25, Number 8, August 2018, Page 902
https://doi.org/10.1007/s12613-018-1639-y

Synthesis and characterization of copper foams through a powder metallurgy route using a compressible and lubricant space-holder material

Mohit Sharma[1,2], *O.P. Modi*[2,3], *and Punit Kumar*[1)]

1) Department of Mechanical Engineering, National Institute of Technology, Kurukshetra, Haryana 136119, India

2) CSIR- Advanced Materials & Processes Research Institute, Bhopal 462026, India

3) Department of Material Science & Metallurgical Engineering, Maulana Azad National Institute of Technology, Bhopal 462003, India

(Received: 20 October 2017; revised: 29 March 2018; accepted: 2 April 2018)

Abstract: In the present work, a compressible and lubricating space-holder material commonly known as "acrawax" was used to process Cu foams with various pore sizes and various porosities. The foams were processed without using binders to avoid contamination of their metal matrices. The lubricant space-holder material was found to facilitate more uniform flow and distribution of metal powder around the surface of the space holder. In addition, the use of acrawax as a space-holder material yielded considerably dense cell walls, which are an essential prerequisite for better material properties. The foams processed with a smaller-sized space holder were found to exhibit better electrical and mechanical properties than those processed with a coarser-sized space holder. The isotropic pore shape, uniform pore distribution throughout the metal matrix, and uniform cell wall thickness were found to enhance the properties pertaining to fine-pore foam samples. The processed foams exhibit properties similar to those of the foams processed through the lost-carbonate sintering process.

Keywords: copper foam; powder metallurgy; space holder; acrawax; flexural strength; sintering; electrical resistivity

1. Introduction

Cu foams have been extensively researched over the past decade owing to their potential applications as electrodes in water filters, and in thermal energy storage and heat transfer devices [1–9]. Among the various techniques [10–14] used to synthesize porous materials, powder metallurgical processing is one of the most widely used [15–26]. One of the processes used in powder metallurgy is the space-holder technique [27–31], where the evaporation of a space holder leaves behind a network of pores within a metal matrix. This technique is relatively easy and efficiently produces the desired porous materials [31].

Several researchers have used various types of space holders, demonstrating their relative advantages over each other. The space-holder materials used in early investigations were mainly water-leachable compounds such as table salt [17–18], sugar [19–20], and urea [21–22]. Another class of space holders is the evaporative type, which includes urea [23], polymethyl methcrylate polymer [32], ammonium hydrogen carbonate [33], and magnesium [26], which volatilize when heated. Sublime compounds such as naphthalene [25] and organic products such as tapioca starch [24] and cellulose fiber [34] have also been used as space-holder materials. The large variety of available space-holder materials makes selection of an appropriate space holder for a given application difficult. In attempts to attain materials with high strength and good energy absorption properties, the space-holder material is expected to play an important role in cell wall densification and uniform pore distribution. Ideally, the space-holder material should not react with the metal matrix or leave behind residues.

NaCl is a widely used space-holder material because it can withstand working temperatures as high as 800°C without decomposing. Ye and Dunand [17] hot pressed Ti and NaCl powders at 780°C under a pressure of 30–50 MPa and then leached the NaCl using hot water. The authors obtained dense cell walls with low microporosity. Their Ti foams exhibited better mechanical properties in terms of strength and energy absorption. Notably, however, hot

Corresponding author: Mohit Sharma E-mail: mohit826@gmail.com

pressing Ti and NaCl together at temperatures of 800°C or greater can lead to contamination of the Ti matrix.

Jakubowicz *et al*. [19] pressed Ti powder and sugar particles using high compaction pressure (500 MPa) and removed the sugar particles immediately after the cold compaction process to avoid any reactions at high temperatures. However, the pores of the processed foams were irregularly shaped because of the poor compressibility of the sugar particles. Here, using a high compaction pressure could not be an appropriate method because of the poor compressibility of the water-leachable compound.

Another space-holder material that can withstand high temperatures is potassium carbonate [35–36]. After cold compaction, metal and potassium carbonate powders are sintered together for 4 h at a high temperature. The potassium carbonate is thereafter leached into water. Because the leaching is performed as the last step, dense cell walls are obtained with this process. However, this process includes long sintering and leaching durations, making it time consuming. Jia *et al*. [37] used an innovative approach of ultrasonic tapping of Ti powder with NaCl beads at a 4-Hz frequency. The author's cold compacted the tapped powder mixture at 450 MPa. Although the ultrasonic tapping process promoted the formation of dense cell walls, the pores were elongated in the direction of compaction, forming ellipsoid pores. Khodaei *et al*. [38] reported similar results for processing Ti foams using high compaction pressures, where the pores were elongated in the direction of pressing. These results suggest that a high compaction pressure is essential for obtaining dense cell walls, but the high pressure ultimately changes the pore/space-holder morphology.

Another possible method for achieving higher strength foams is to add binders such as polyvinyl alchohol or sodium silicate along with the space-holder material. The binders help in holding the weak metal matrix after the space holder is removed. In addition, the binders reduce the friction among powder particles during cold compaction and intensify the binding among particles. However, binders tend to leave residues/precipitates, which adversely affect the properties of the obtained foam. Wang and Zhang [32] studied the effect of using binders on the impurities and sintering behavior of foams. The authors suggested using minimal amounts of binders to achieve dense cell walls and reduce impurities. Hence, we inferred from the aforementioned discussion that, although using a high compaction pressure is essential for high-strength foams, the space holder should be compressible enough to sustain high pressures. In addition, if low compaction pressures are used, then binders become essential, ultimately hindering the sinterability of the foam. Therefore, a need exists to find an optimal solution to these two general problems encountered in processing foams using the space-holder technique.

The main objective of the present work is to process foams without binders using moderate compaction pressure and a space-holder material that is itself a lubricant. The idea underlying the use of a lubricating space-holder material is that the metal powders can flow easily around the space holder and facilitate better cohesion between metal powder particles at moderate compaction pressures. Recently, Ti [39–40] and Cu foams [41] have been synthesized using such a space holder, i.e., acrawax, which is commonly used as a lubricant in powder metallurgical processing of aluminum alloys. It exhibits excellent lubrication properties and is readily removed without leaving any residue. Moreover, very little literature [39–41] is available on the use of acrawax as a space holder and its effect on the metal foam properties. In the present work, as-received acrawax was sieved in two size ranges, i.e., <500 μm and 500–1100 μm. This work discusses the potential use of acrawax as a better space-holder material for obtaining high-quality foams. Both electrical as well as mechanical properties of the developed Cu foams are investigated.

2. Experimental

Cu powder (average particle size of about 45 μm and purity of 99.5%) supplied by Alfa Aesar (Fig. 1(a)), USA, acrawax coarse particles (Fig. 1(b)) (particle size range: 500–1100 μm, 99.5% pure), and acrawax fine particles (Fig. 1(c)) (particle size range: <500 μm) supplied by Lonza, USA were used as the raw materials. Acrawax melts at approximately140–145°C and is chemically known as *N*, *N*′-ethylene bis(stearamide) [41]. Previous studies [41] have shown that acrawax evaporates and leaves no residues. The density of acrawax has been reported to be approximately 1 g/cm^3.

Cu powder was mixed with various quantities of acrawax (both fine and coarse particles) to obtain Cu foams with porosities in the range from 40vol% to 70vol%. The foams processed using coarse and fine particles of acrawax are hereafter referred to as foams with coarse pores and foams with fine pores, respectively. After uniform mixing, each powder mixture was cold compacted using a single-action hydraulic press in a 10-mm-diameter cylindrical die at a pressure of 300 MPa. The cold-compacted samples were then heated at 350°C for 2 h in a tube furnace (Ar atmosphere) to completely remove acrawax, as was confirmed by reweighing the pre-heated compacts. This treatment leading

to the dissociation of acrawax is referred to here as pre-heating, and the obtained samples are referred to as pre-heated samples. The pre-heated powder compacts were then finally sintered in a tube furnace under an Ar atmosphere for 60 min at 900°C. The heating rate during sintering was 10°C/min. The density of the sintered samples was calculated by weight and volume measurement of the final sintered samples, and the results were compared with the theoretical density of Cu (8.96 g/cm^3). The pore morphology was examined using a field-emission scanning electron microscope (FE-SEM) supplied by FEI, USA and equipped with an energy-dispersive spectroscopy (EDS) apparatus from Oxford Instruments, UK. The pores obtained through the dissolution of acrawax and the pores present in the cell wall are referred to here as "macropores" and "micropores", respectively. The foam samples for flexural testing (three-point bending) and electrical resistivity measurements were prepared using a die with rectangular dimensions (length = 31 mm, width = 12.5 mm). The flexural tests were conducted using a span length of 25 mm, and the speed of deformation was maintained at 1 mm/min. Compression testing of the foam samples was carried out at a strain rate of 0.001 s^{-1} using an Instron 8801 UTM. The electrical resistivity of rectangular samples was measured by a micro-ohmmeter supplied by Sivananda Electronics, India. The four-probe method was used to determine the electrical resistivity of the rectangular specimens.

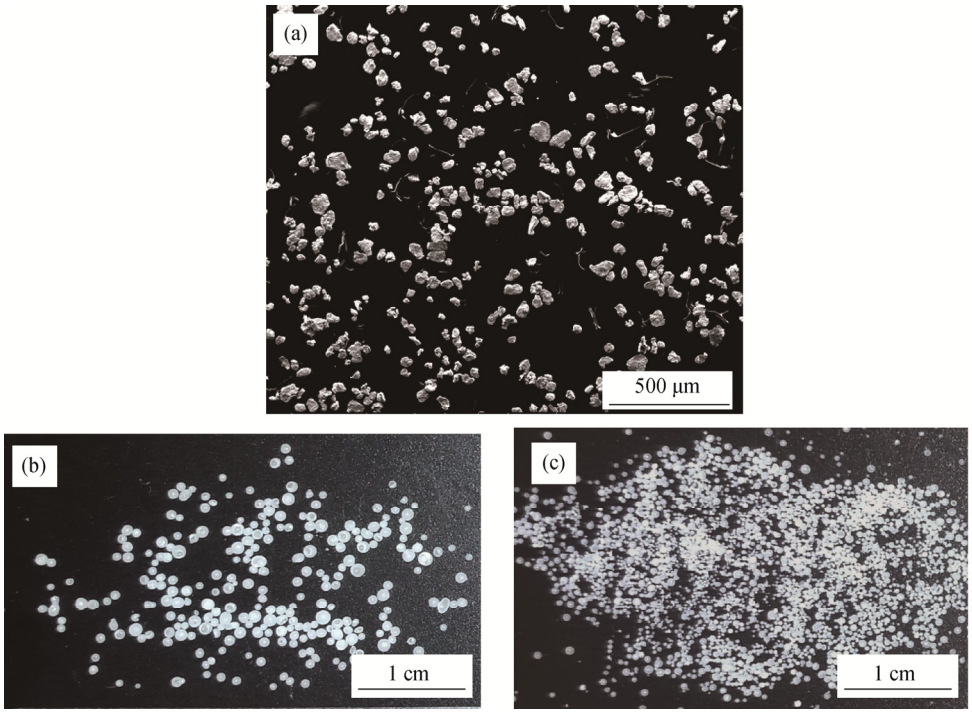

Fig. 1. Starting raw materials: (a) SEM image of copper powder particles; (b) acrawax sieved in the range 500–1100 μm; (c) acrawax sieved in the range <500 μm.

3. Results and discussion

3.1. Effect of compaction pressure on pore morphology

One of the prime objectives of this study is to attain dense cell walls without compromising the pore morphology. The selection of an appropriate compaction pressure is important to obtain high-strength foams. To evaluate the effect of compaction pressure on pore morphology and densification, three compaction pressures (200, 300, and 400 MPa) were initially chosen. Figs. 2(a) and 2(b) show SEM images of the foams processed using 200, 300, and 400 MPa compaction pressures. The foam samples processed using 200 MPa pressure (Fig. 2(a)) is found to have spherical pores; however, the cell walls obtained here are porous (micropores indicated by arrows). The cell walls were denser in the foam compacted at 300 MPa (Fig. 2(b)) than in that compacted at 200 MPa. Also, the pores of the foam compacted at 300 MPa are mostly spherical. The cell walls in the samples compacted at 400 MPa are dense; however, the high pressure led to deformation of the pore morphology into an ellipsoidal shape. The pores obtained are in contrast to the spherical shape of acrawax particles. Notably, howev-

er, the aforementioned deformation of acrawax occurred without fracture, and the shape of the obtained pores was that of the deformed acrawax. Hence, acrawax exhibited compressible behavior, and high pressures deformed it into an elliptical shape. Because the major objective of the present work was to achieve dense cell walls without excessive deformation of acrawax, we opted to use the average of the two compaction pressures (i.e., 300 MPa).

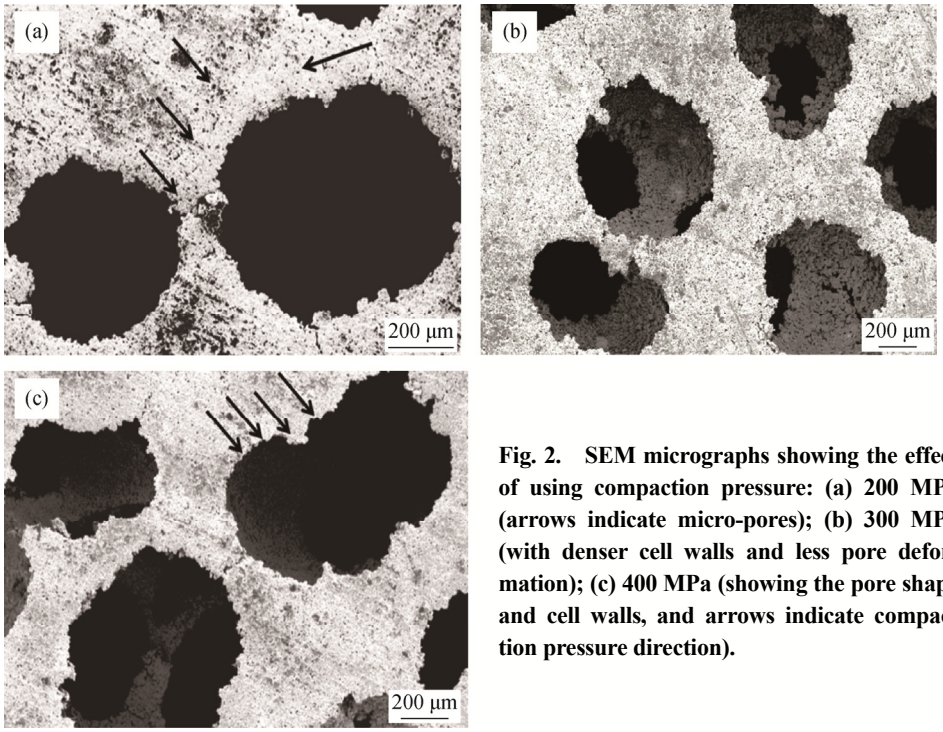

Fig. 2. SEM micrographs showing the effect of using compaction pressure: (a) 200 MPa (arrows indicate micro-pores); (b) 300 MPa (with denser cell walls and less pore deformation); (c) 400 MPa (showing the pore shape and cell walls, and arrows indicate compaction pressure direction).

3.2. Effect of acrawax addition on the final porosity obtained in foams

The foam samples with various acrawax contents (both fine and coarse acrawax) ranging from 40vol% to 70vol% were processed at 300 MPa compaction pressure. Table 1 shows the effect of the added space holder on the final achieved porosity in the cases of both fine and coarse-pore foam samples. The copper foams with finer pores are designated as CF1, CF2, CF3, and CF4 and the coarser-pore foams as CF5, CF6, CF7, and CF8.

Table 1. Sample dimensions and final porosity achieved after the sintering process for samples with various acrawax contents

Copper foam	Amount of space holder added		Weight (after pre-heating), W_p / g	Weight (after sintering), W_s / g	Diameter (after pre-heating), D_p / mm	Diameter (after sintering), D_s / mm	Height (after pre-heating), H_p / mm	Height (after sintering), H_s / mm	Final porosity / %
	Volume fraction / %	Weight fraction / %							
CF1	40	6.8	2.9	2.7	10	9.5	10.5	10.1	57.8
CF2	50	9.7	2.8	2.6	10	9.5	10.8	10.0	58.5
CF3	60	13.9	2.8	2.5	10	9.2	12.1	11.2	62.2
CF4	70	20.1	2.7	2.2	10	9.2	13.3	12.2	69.8
CF5	40	6.8	2.9	2.8	10	8.9	12.1	11.0	54.0
CF6	50	9.7	3.1	2.8	10	9.1	13.2	11.7	57.8
CF7	60	13.9	2.9	2.7	10	9.5	11.7	11.3	62.7
CF8	70	20.1	3.0	2.8	10	10.3	14.4	14.3	73.8

In all the samples, the final porosity was greater than the space-holder content when the added amount of space holder was 40vol%. This result suggests that extra porosity may be present as micropores within the cell walls or as some cracks around the periphery of the pores. However, when the space-holder content was increased to 60vol% and 70vol%,

the final porosity matched with content of added space-holder. Other authors [26,41] have reported that foams with pore contents >55% form interconnected channels of pores. Hence, when more space holder is added, the pores formed after evaporation of acrawax begin to form an interconnected network, facilitating easier and complete removal of the acrawax. However, the situation differs substantially for low-porosity samples, where the acrawax vapor lacks easy passage because of lesser interconnectivity and isolated pores. The cell walls around the evaporating acrawax are also dense because of the use of high compaction pressure. Consequently, cracks are formed around the pores because of the excessive vapor pressure of the acrawax and the generation of micropores within the cell walls themselves [41].

The difference between the space-holder content and porosity was greater for coarser acrawax than for finer acrawax. This greater difference is easily explained by the larger quantity of pores in the finer acrawax for the same pore volume. Hence, the pore connectivity is better when fine-sized acrawax is used, which facilitates easy removal without generating any cracks or micropores.

3.3. Pore morphology and distribution

To observe the pore distribution in the matrix, we cut the samples along the thickness cross-sections (Fig. 3). Figs. 4(a) and 4(b) show the foam samples with fine pores cut along the centerline (A) (center) and the other near the edge line (B) (side) of the thickness cross-section (Fig. 3). The 50% porous samples (Fig. 4(a)) have both densified (marked by arrows) as well as porous regions present along the thickness cross-section. The region near the edges (side) and central region sinter at a faster rate because of small-sized pores obtained using finer acrawax. In addition, the pores in the central and side regions of the thickness cross-section were smaller, irrespective of the size of acrawax used. These smaller pores are attributed to the self-diffusion phenomenon being more predominant because of the small size of the pores. High-porosity samples (Fig. 4(b)) have similar pore volumes and sizes in both the central and edge (side) regions. Here, we inferred that the increased pore connectivity led to more uniform sintering/shrinking of the pores irrespective of their location in the metal matrix.

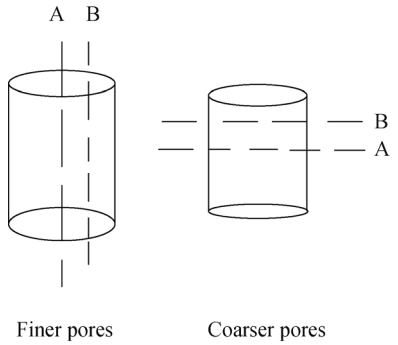

Fig. 3. Cutting direction shown by lines A (central area) and B (side area) in the case of fine and coarser pores.

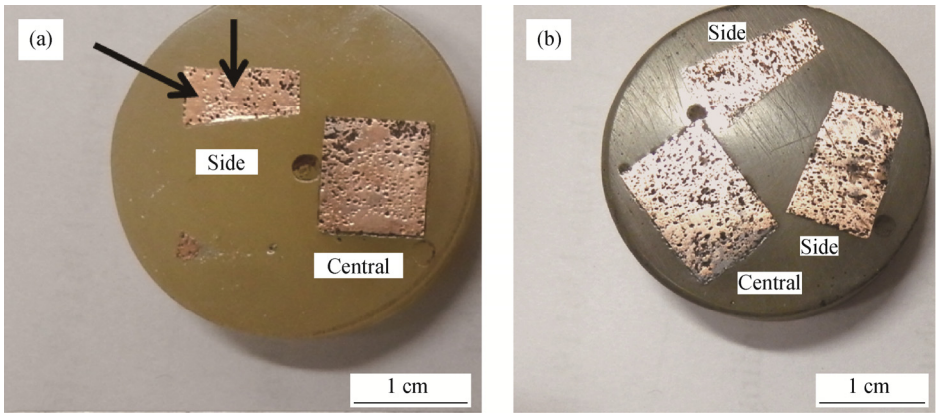

Fig. 4. Optical photographs of fine pore foam samples cut longitudinally: (a) 50% porous (arrows show full densified areas); (b) 70% porous showing uniform pore distribution both in central and side regions.

The foam samples with coarser pores were cut horizontally (Fig. 5) because they tend to fracture when cut vertically. The central regions (A) (Fig. 5(a)) of these samples contain much fewer pores than the central regions of the foam samples with finer pores. This difference in the number of pores is attributed the larger-sized pores occupying more volume while present in a smaller area compared with the finer pores. The foams with higher porosity (Fig. 5(b)) are found to have more uniform pore distribution in the central and edge regions. Accordingly, we inferred that interconnectivity of the pores plays a major role in the sintering process for both fine and coarse-pore samples. As the pores become more interconnected, the pore size and distribution become more uniform. Also, the fine-pore samples exhibit a more uniform pore size distribution and greater strength compared with the coarse pores, even in the lower-porosity samples (40% porosity).

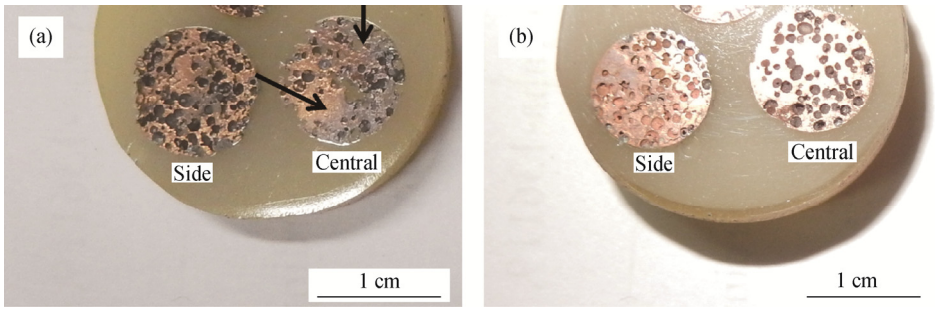

Fig. 5. Optical photographs of coarse pore foam samples cut horizontally: (a) 50% porous (arrows show full densified areas); (b) 70% porous having uniform pore distribution in both central and side regions.

3.4. SEM and EDS analysis of Cu foam

Fig. 6(a) shows the fine-pore samples with a uniform distribution of the pores in the metal matrix. Higher-magnification observations of the foam samples revealed that the cell wall regions also contain some micropores (Fig. 6(b)). The microporosity in the cell walls was attributed to the varied size of the fine acrawax (<500 μm) shown in Fig. 1(c). Some of the acrawax particles in the finer acrawax are observed to be very fine (10–20 μm). These fine powders have possibly dispersed in the cell wall regions and created microporosity in the cell walls. However, the micropores present in the cell walls are small and the pore size is between 5 to 20 μm. Furthermore, the cell walls have a uniform cell wall thickness in this case. The pores, being smaller in size, are present in a larger volume; hence, a more uniform cell wall thickness is achieved in the fine-pore foams. Figs. 7(a) and 7(b) show SEM images of the foam after sintering in the case of coarse-pore samples (60vol% porosity). These images show that the cell walls densified well, with lesser microporosity present in the cell walls. However, here the cell walls are of variable thicknesses across the foam surface compared to fine-pore samples (Fig. 6(a) vs. Fig 7(a)). The variation in cell wall thickness decreased substantially and became more uniform when the porosity increased to 70vol%. Another important observation was the roundness of the pores after sintering. The

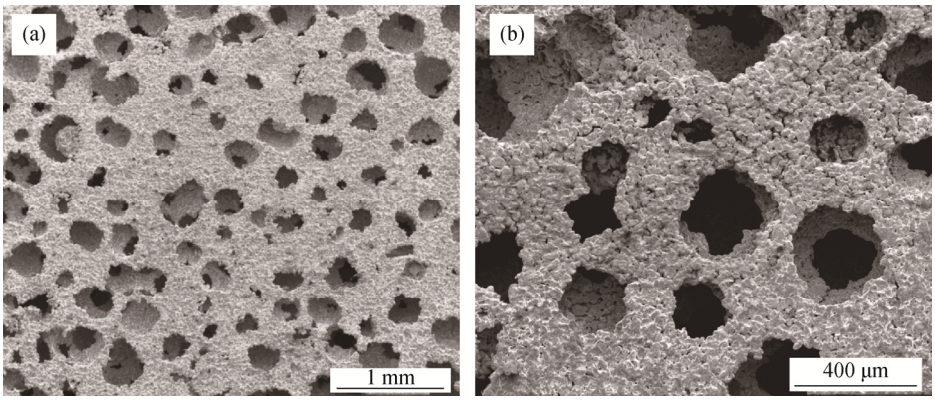

Fig. 6. SEM micrographs of 60vol% porous foams with finer pores showing the pore distribution (a) and cell walls (b).

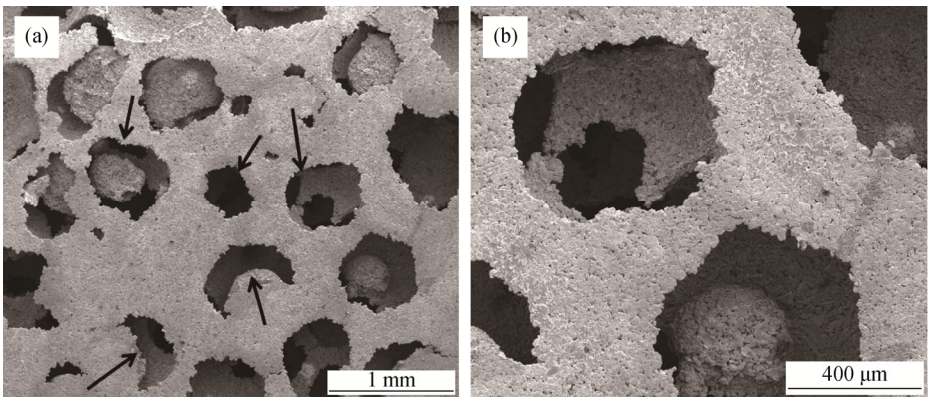

Fig. 7. SEM micrographs of 60vol% porous foams with coarser pores showing the pore distribution (a) and cell walls (b).

fine-pore samples have a larger number of round pores compared with the coarser-pore samples (Fig. 6(a) vs. Fig 7(a)). The deformed pores (non spherical shape) are marked by arrows (Fig. 7(a)) to show their deformation in the compaction direction.

Notably, the cell walls (struts) obtained in the case of fine and coarse-pore samples are continuous and dense (with less microporosity). The continuity in strut formation is achieved during the compaction process, where the metal powder has to flow uniformly around the space-holder material. When uniform flow is achieved, then the chance of forming dense struts with less microporosity is enhanced. To obtain dense and continuous struts, Parvanian and Panjepour [16] used mechanically activated Cu powder instead of normal Cu powder for efficient packing around the space holder they used, i.e., potassium carbonate, which is a non-lubricant. However, in our case, even using normal Cu powder led to the formation of continuous and dense struts (Figs. 6 and 7) because of the lubricant nature of acrawax.

To investigate the impurities that might have been left behind after evaporation of the acrawax, we conducted EDS analysis of the foams. Fig. 8 shows two EDS spectra corresponding to the point on the cell wall and the other at the pore periphery. Here, no impurities were present except for some oxidation (Table 2). The oxidation was less extensive in the cell wall regions and only slightly more extensive at the pore periphery. We therefore concluded from the EDS results that acrawax was volatilized completely without leaving any impurities within the metal foam matrix.

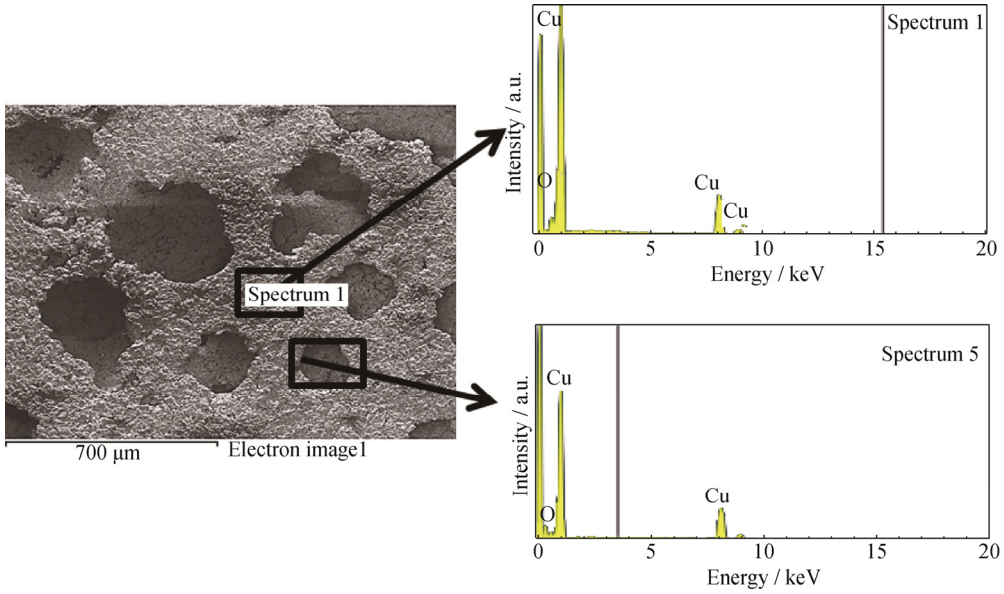

Fig. 8. EDAX spectra of copper foams near the pore periphery and on the cell wall showing presence of only copper and oxygen.

Table 2. EDS elemental analysis results for different areas of Cu foams wt%

Location	Copper	Oxygen
On the periphery of pore	95.91	4.09
Cell wall region	96.01	3.99

3.5. Mechanical and electrical properties of foam

The mechanical properties of the foam were tested using flexural tests. The flexural strength (F_s) of a beam was calculated using the following formula:

$$F_s = \frac{3PL}{2wt^2},$$

where P is the load before failure, L is the length of the span, w is the width of the sample, and t is the thickness of the sample.

Table 3 lists the values of the width, thickness, load, and flexural strength along with the specific flexural strength (i.e., the F_s/density (ρ) ratio) for the samples. The foam samples with finer pores exhibit greater flexural strength compared with the coarser-pore samples. The F_s/ρ ratio for the fine-pore foam samples (60vol%, 70vol% porosity) was found to be equivalent to that of Cu foams processed using the lost-carbonate sintering process with similar pore size and volume [16]. Interestingly, only the samples with a pore content greater than 60% exhibit reasonably good F_s values, which suggests that pore interconnectivity enhances the F_s. The isolated pores in the low-porosity (<60%) samples act as stress concentration sites, leading to sudden/cascade failure of the foams. Table 3 shows that the F_s values of the fine-pore foams with 60vol% and 70vol% porosity are 25 MPa and 10 MPa, with flexural strain values at 2.58% and 2.6%, respectively.

Table 3. Flexural strength, density, and dimensions of rectangular-shaped Cu foams prepared with fine and coarse pores

Copper foam	Width / mm	Length / mm	Thickness / mm	Density, ρ / ($g \cdot cm^{-3}$)	Flexural strength, F_s / MPa	Specific flexural strength, (F_s/ρ)	Flexural strain / %
CF1	12.5	30.7	3.4	3.8	4	1.1	1.7
CF2	12.2	30.2	3.5	3.7	18	4.8	1.2
CF3	12.2	30.4	3.6	3.4	25	7.4	2.8
CF4	12.0	30.2	4.2	2.6	10	3.8	2.6
CF5	12.6	31.4	3.7	4.1	7	1.7	1.3
CF6	12.7	31.4	3.7	3.8	5	1.3	0.8
CF7	12.7	31.5	4.3	3.3	5	1.5	1.9
CF8	12.7	31.5	4.2	2.3	5	2.2	1.8

The F_s values of the coarser-pore samples are quite low (approximately 5 MPa) in the cases of 60vol% and 70vol% porosity. The lower strength in the case of the coarser-pore samples is attributed to the difference in cell wall thickness and pore size in various regions across the thickness cross-section. The presence of larger pores favors crack initiation and hence lowers the F_s value. However, the samples undergo substantial flexural extension before fracture.

The fractured surfaces of the samples after flexural testing were observed by SEM. The fractured surfaces of the fine-pore samples mostly exhibit ductile fracture (Fig. 9(a)). Here, the cracks are not formed in and around the pores (Fig. 9(b)). Hence, the samples showed much higher F_s values than the coarser-pore samples. Therefore, we concluded that finer pores are associated with uniform cell wall thickness, pore size, and pore distribution throughout the cross-section, which, in turn, leads to higher F_s values. Notably, the microporosity in the cell walls did not strongly affect the F_s of the fine-pore foams.

Fig. 10(a) shows the fractured surface of the coarser-pore sample with 70vol% porosity. Cracks developed (marked by arrows) wherever the cell walls are relatively thinner. Fig. 10(b) shows two pores in close proximity to each other. Because of this close proximity, the cell wall separating the pores is narrow, leading to crack initiation in one of the pores. We concluded that the thickness of cell walls is one of the most important factors controlling the failure mode as well as the F_s.

Fig. 11 shows the compressive stress–strain diagram of the foam samples. Both the fine- and coarse-pore samples show a distinct plateau region in the 60vol% and 70vol% porosity samples, followed by densification. The fine-pore samples demonstrated greater plateau strengths of 15 and 5 MPa. The coarse-pore samples showed yield strengths of 10 and 4 MPa followed by a sudden decrease of the stress values. However, in both cases, a distinct deformation was observed before the densification region started. The plateau region deformation was nearly 40% and 50% for the fine- and coarse-pore samples, respectively, similar to the plateau region of foams processed via the lost-carbonate sintering process [35]. Also, the compressive plateau/yield strength was approximately 4 MPa (70vol% porosity) for both the fine- and coarse-pore samples. This strength is substantially greater than that of the Cu foams (strength less than 1 MPa) with a similar porosity produced via the lost-carbonate process [36].

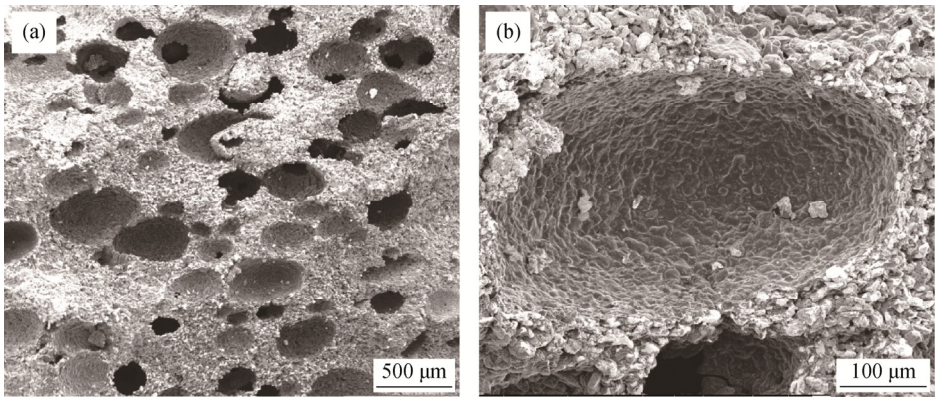

Fig. 9. SEM images of the fractured surface obtained after flexural testing of 70vol% porous samples (a) and magnified image of a pore (b).

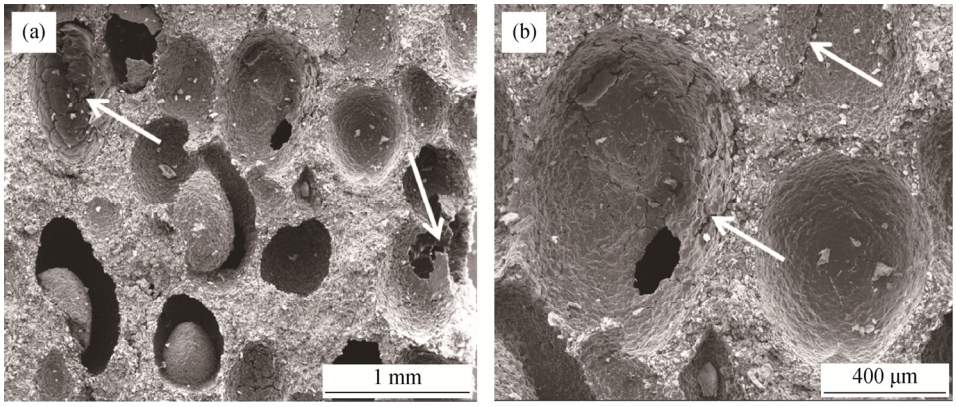

Fig. 10. SEM images of the fractured surface obtained after flexural testing of 70vol% porous samples with coarse pores (arrows depicting the cracks formed after testing in and around the pores) (a) and magnified image of the pore (b).

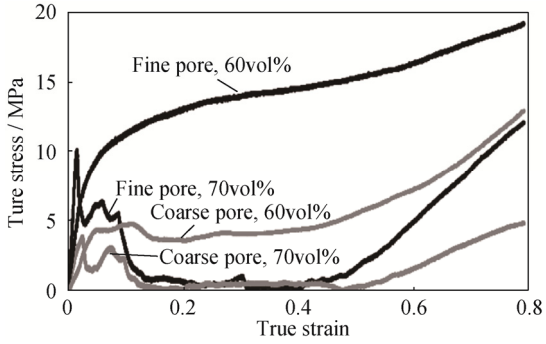

Fig. 11. True compressive stress-strain diagram of the coarse and fine pore foam samples.

Fig. 12 shows the electrical resistivities of foams for both coarse- and fine-pore samples. The coarse-pore samples show relatively high electrical resistivities for the same pore volume. The electrical resistivity of the 40vol% samples (CF4) is much higher than the resistivities of the other samples. The resistivities of both the fine-and coarse-pore samples show increasing resistivity values with increasing porosity (50vol%–70vol%)—a general behavior observed for most of the metallic foams.

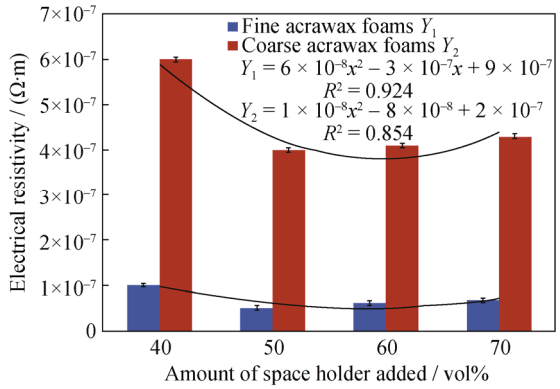

Fig. 12. Electrical resistivity of fine and coarse pore foam samples varying with the added space holder content.

Importantly, the coarse-pore samples have much higher electrical resistivity values in all of the investigated cases when compared with fine-pore samples. This observation is contrary to the results of an earlier study [42], wherein smaller pores led to higher electrical resistivity in Ti foams. This behavior was attributed to a particular area containing a greater number of pores and generating stronger interacting electric fields, which increases the resistivity of small-sized pores [42]. However, in the present work, the samples with finer-sized pores show lower resistivity than the samples with coarser-sized pores, which we attribute to several possible causes. For the same pore volume, small-sized space-holder particles were present in greater numbers than large-sized space-holder particles. The pores were more isotropic in shape and were present more uniformly throughout the thickness cross-section. However, in the coarse-pore samples, the distribution of pores was less uniform, especially in the low-porosity samples. This poor uniformity led to opposing/interacting electrical fields generated in solid versus porous areas. This interpretation is further strengthened by the observation that sample CF4 exhibits much higher resistivity than sample CF1. Because the processing conditions of both types of foams is similar, the only difference that can reasonably explain the aforementioned observations is the larger number of pores present in the fine-pore samples, which led to a more uniform pore distribution and to better interconnectivity of the pores. In the CF4 sample, some regions contain pores and some regions are dense, which generates greater electrical interferences in low-porosity samples.

Uniform cell wall thickness could be another factor controlling the electrical resistivity. The uniform cell walls provided better conducting pathways compared with the case of irregular cell wall thicknesses in the coarse-pore samples. In addition, the pores obtained in the case of fine-pore samples

are more spherical (Fig. 6(a)). The coarser-pore samples, however, have various shape and are less spherical in shape (Figs. 7(a) and 8). If we consider the pore aspect ratio (i.e., the ratio between the length of the major axis and that of the minor axis) after an equivalent compression, larger spheres/pores will have higher aspect ratios than smaller spheres/pores. As demonstrated in earlier studies, the electrical conductivity is more dependent on the pore shape than on the pore size. Li and Lu [42] suggested that, when the pores have a high aspect ratio (being shorter along the pressing direction and longer in the perpendicular direction), the resistivity is much higher, as observed in our case of coarse-pore samples.

The aforementioned possibilities might have enhanced the electrical resistivity of the fine-pore foam samples. In addition, although the microporosity was greater in the case of the fine-pore samples, it did not strongly affect the resistivity. We thus concluded on the basis of the preceding discussion that uniformity in pore distribution throughout the thickness cross-section, a spherical pore shape, and a uniform cell wall thickness are dominant factors compared with pore size in influencing the electrical properties of Cu foams.

4. Conclusions

The space-holder material acrawax was used to process Cu foams with various pore contents and sizes. High compaction pressures were beneficial for obtaining dense cell walls in the prepared foams. However, the compaction pressure used herein was limited to avoid excessive deformation of acrawax from spherical to ellipsoid shape. The mechanical and electrical properties obtained using fine acrawax were found to superior to those obtained using coarse acrawax. For comparable values of compaction pressure and pore volume, the fine acrawax yields more isotropic pores as compared with those obtained with coarse acrawax. The shrinkage and densification of pores during sintering were found to be more uniform for the case of fine pores. The pore size, pore shape, and cell wall thickness were found to be more variable in the case of the coarse-pore samples. The electrical properties of fine-pore samples were found to be much better than those of coarse-pore samples because the fine-pore samples exhibit better uniformity in pore distribution throughout the thickness cross-section, a spherical pore shape, and a uniform cell wall thickness. Further, the fine-pore foams processed using acrawax showed properties similar to those of foams processed via the lost-carbonate sintering process.

Acknowledgements

The first author wishes to thank the Director, CSIR-Advanced Materials and Processes Research Institute, Bhopal, Dr. O.P. Modi and Mr. G.K. Gupta, CSIR-AMPRI, Bhopal for making this work possible.

References

[1] N. Dukhan, *Metal Foams: Fundamentals and Applications*, DEStech Publications, Pennsylvania, USA, 2012, p. 381.

[2] R. Goodall, *Porous Metals: Foams and Sponges*, [in] *Advances in Powder Metallurgy: Properties*, *Properties and Applications*, Woodhead publishing limited, Oxford, 2013, p. 273.

[3] F. Stergioudi, E. Kaprara, K. Simeonidis, D. Sagris, M. Mitrakas, G. Vourlias, and N. Michailidis, Copper foams in water treatment technology: removal of hexavalent chromium, *Mater. Des.*, 87(2015), p. 287.

[4] H. Jo, Y. Cho, M. Choi, J. Cho, J.H. Um, Y. Sung, and H. Choe, Novel method of powder-based processing of copper nanofoams for their potential use in energy applications, *Mater. Chem. Phys.*, 145(2014), No. 1-2, p. 6.

[5] A. Etiemble, J. Adrien, E. Maire, H. Idrissi, D. Reyter, and L. Roué, 3D morphological analysis of copper foams as current collectors for Li-ion batteries by means of X-ray tomography, *Mater. Sci. Eng. B*, 187(2014), p. 1.

[6] W. Lu, C.Y. Zhao, and S.A. Tassou, Thermal analysis on metal-foam filled heat exchangers. Part I: Metal-foam filled pipes, *Int. J. Heat Mass Trans.*, 49(2006), No. 15-16, p. 2751.

[7] J.M. Baloyo, Open-cell porous metals for thermal management applications: fluid flow and heat transfer, *J. Mater. Sci. Technol.*, 33(2017), No. 3, p. 265.

[8] C. Moon, D. Kim, G.B. Abadi, S.Y. Yoon, and K.C. Kim, Effect of ligament hollowness on heat transfer characteristics of open-cell metal foam, *Int. J. Heat Mass Trans.*, 102(2016), p. 911.

[9] X.H. Liu, H.Y. Huang, and J.X. Xie, Effect of strain rate on the compressive deformation behaviors of lotus-type porous copper, *Int. J. Miner. Metall. Mater.*, 21(2014), No. 7, p. 687.

[10] M.F. Ashby, T. Evans, N.A. Fleck, L.J. Gibson, J.W. Hutchinson, and H.N.G. Wadley *Metal Foams: A Design Guide*, Butterworth Heinemann, USA, 2000, p. 6.

[11] J. Banhart, Manufacture, characterisation and application of cellular metals and metal foams, *Prog. Mater. Sci.*, 46(2001), No. 6, p. 559.

[12] D.C. Dunand, Processing of titanium foams, *Adv. Eng. Mater.*, 6(2004), No. 6, p. 369.

[13] M. Garcia-Avila and A. Rabiei, Effect of sphere properties on microstructure and mechanical performance of cast composite metal foams, *Metals*, 5*(*2015), No. 2, p. 822.

[14] M. Garcia-Avila, M. Portanova, and A. Rabiei, Ballistic performance of composite metal foams, *Compos. Struct.*, 125(2015), p. 202.

[15] A.M. Parvanian, M. Saadatfar, M. Panjepour, A. Kingston, and A.P. Shepperd, The effects of manufacturing parameters on geometrical and mechanical properties of copper foams produced by space holder technique, *Mater. Des.*, 53(2014), p. 681.

[16] A.M. Parvanian and M. Panjepour, Mechanical behavior improvement of open-pore copper foams synthesized through space holder technique, *Mater. Des.*, 49(2013), p. 834.

[17] B. Ye and D.C. Dunand, Titanium foams produced by solid-state replication of NaCl powders, *Mater. Sci. Eng. A*, 528(2010), No. 2, p. 691.

[18] N. Jha, D.P. Mondal, J.D. Majumdar, A. Badkul, A.K. Jha, and A.K. Khare, Highly porous open cell Ti-foam using NaCl as temporary space holder through powder metallurgy route, *Mater. Des.*, 47(2013), p. 810.

[19] J. Jakubowicz, G. Adamek, and M. Devidar, Titanium foam made with saccharose as a space holder, *J. Porous Mater.*, 20(2013), No. 5, p. 1137.

[20] N. Michailidis, F. Stergioudi, A. Tsouknidas, and E. Pavlidou, Compressive response of Al-foams produced via a powder sintering process based on a leachable space-holder material, *Mater. Sci. Eng. A*, 528(2011), No. 3, p. 1662.

[21] N. Bekoz, and E. Oktay, Effects of carbamide shape and content on processing and properties of steel foams, *J. Mater. Process. Technol.*, 212(2012), No. 10, p. 2109.

[22] D.R. Tian, Y.H. Pang, L. Yu, and L. Sun, Production and characterization of high porosity porous Fe–Cr–C alloys by the space holder leaching technique, *Int. J. Miner. Metall. Mater.*, 23(2016), No. 7, p. 793.

[23] M. Sharma, G.K. Gupta, O.P. Modi, B.K. Prasad, and A.K. Gupta, Titanium foam through powder metallurgy route using acicular urea particle as space holder, *Mater. Lett.*, 65(2011), No. 21-22, p. 3199.

[24] A. Mansourighasri, N. Muhamad, and A.B. Sulong, Processing titanium foams using tapioca starch as a space holder, *J. Mater. Process. Technol.*, 212(2012), No. 1, p. 83.

[25] Y.M.Z. Ahmed, M.I. Riad, A.S. Sayed, M.K. Ahlam, and M.E.H. Shalabi, Correlation between factors controlling preparation of porous copper via sintering technique using experimental design, *Powder Technol.*, 175(2007), No. 1, p. 48.

[26] Z. Esen and S. Bor, Processing of titanium foams using magnesium spacer particles, *Scripta Mater.*, 56(2007), No. 5, p. 341.

[27] I. Mutlu, S. Yeniyol, and E. Oktay, Production and precipitation hardening of beta-type Ti–35Nb–10Cu alloy foam for implant applications, *J. Mater. Eng. Perferm.*, 25(2016), No. 4, p. 1586.

[28] B. Arifvianto and J. Zhou, Fabrication of metallic biomedical scaffolds with the space holder method: a review, *Materials*, 7(2014), No. 5, p. 3588.

[29] M. Khodaei, M. Meratian, and O. Savabi, Effect of spacer type and cold compaction pressure on structural and mechanical properties of porous titanium scaffold, *Powder Metall.*, 58(2015), No. 2, p. 152.

[30] V. Amigó, L. Reig, D.J. Busquets, J.L. Ortiz, and J.A. Calero, Analysis of bending strength of porous titanium processed by space holder method, *Powder Metall.*, 54(2011), No. 1, p. 67.

[31] M. Sharma, G.K. Gupta, O.P. Modi, and B.K. Prasad, PM processed titanium foam: influence of morphology and content of space holder on microstructure and mechanical properties, *Powder Metall.*, 56(2013), No. 1, p. 55.

[32] B. Wang and E. Zhang, On the compressive behaviour of sintered porous coppers with low-to-medium porosities-Part II: Preparation and microstructure, *Int. J. Mech. Sci.*, 50(2008), No. 3, p. 550.

[33] J.Y. Xiong, Y.C. Li, X.J. Wang, P.D. Hodgson, and C.E. Wen, Titanium-nickel shape memory alloy foams for bone tissue engineering, *J. Mech. Behav. Biomed. Mater.*, 1(2008), No. 3, p. 269.

[34] Y. Kanoko, K. Ameyama, S. Tanaka, and B. Hefler, Production of ultra-thin porous metal paper by fibre space holder method, *Powder Metall.*, 57(2014), No. 3, p. 168.

[35] M.A. El-Hadek and S. Kaytbay, Mechanical and physical characterization of copper foam, *Int. J. Mech. Mater. Des.*, 4(2008), No. 4, p. 63.

[36] Y.Y. Zhao, T. Fung, L.P. Zhang, and F.L. Zhang, Lost carbonate sintering process for manufacturing metal foams, *Scripta Mater.*, 52(2005), No. 4, p. 295.

[37] J.G. Jia, A.R. Siddiq, and A.R. Kennedy, Porous titanium manufactured by a novel powder tapping method using spherical salt bead space holders: characterisation and mechanical properties, *J. Mech. Behav. Biomed. Mater.*, 48(2015), p. 229.

[38] M. Khodaei, M. Meratian, O. Savabi, and M. Razavi, The effect of pore structure on the mechanical properties of titanium scaffolds, *Mater. Lett.*, 171(2016), p. 308.

[39] D.P. Mondal, M. Patel, S. Das, A.K. Jha, H. Jain, G. Gupta, and S.B. Arya, Titanium foam with coarser cell size and wide range of porosity using different types of evaporative space holders through powder metallurgy route, *Mater. Des.*, 63(2014), p. 89.

[40] D.P. Mondal, M. Patel, H. Jain, A.K. Jha, S. Das, and R. Dasgupta, The effect of particle shape and strain rate on microstructure and compression deformation response of pure Ti-foam made using acrowax as space holder, *Mater. Sci. Eng. A.*, 625(2015), p. 331.

[41] M. Sharma, O.P. Modi, and P. Kumar, Experimental modelling of copper foams processed through powder metallurgy route using a compressible space holder material, *J. Porous Mater.*, 24(2017), No. 6, p. 1581.

[42] B.Q. Li and X. Lu, The effect of pore structure on the electrical conductivity of Ti, *Transp. Porous Media*, 87(2011), No. 1, p. 179.